Preferred Orientations of His64 in Human Carbonic Anhydrase II[†]

C. Mark Maupin and Gregory A. Voth*

Center for Biophysical Modeling and Simulation, and Department of Chemistry, University of Utah, Salt Lake City, Utah 84112-085

Received October 18, 2006; Revised Manuscript Received December 1, 2006

ABSTRACT: Histidine at position 64 (His64) in human carbonic anhydrase II (HCA II) is believed to be the proton acceptor in the hydration direction and the proton donor in the dehydration direction for the rate-limiting proton transfer (PT) event. Although the biochemical effect of histidine at position 64 has been thoroughly investigated, the role of its orientation in the PT event is a topic of considerable debate. X-ray data of HCA II suggests that His64 can adopt either an "in" or "out" orientation. The "in" orientation is believed to be favored for the hydration direction PT event because the N_δ of His64 is closer to the catalytic zinc. This orientation allows for smaller water bridges, which are postulated to be more conducive to PT. In the present work, classical molecular dynamics simulations have been conducted to elucidate the role that the His64 orientation may play in its ability to act as a proton donor/acceptor in HCA II. The free energy profile for the orientation of His64 suggests that the histidine will adopt an "in" orientation in the hydration direction, which brings N_δ in close proximity to the catalytic zinc. When the histidine becomes protonated, it then rotates to an "out" orientation, creating a more favorable solvation environment for the protonated His64. In this "out" orientation, the imidazole ring releases the delta nitrogen's excess proton into the bulk environment. After the second PT event and when the zinc-bound water is regenerated, the His64 is again favored to reorient to the "in" orientation, completing the catalytic cycle.

One of the most extensively characterized enzymes that utilizes a proton transfer (PT) event is carbonic anhydrase (CA) (*1*−*10*). CA, one of the most efficient enzymes known, catalyzes the conversion of carbon dioxide to bicarbonate and an excess proton (*1*, *11*, *12*).

$$CO_2 + H_2O \leftrightarrow H^+ + HCO_3^- \quad (1)$$

CA is key to the transport of CO_2 and can be found in plants, animals, and certain bacteria. In humans, CA is fundamental to CO_2 transport, gluconeogenesis, ureogenesis, and bicarbonate buffering.

Human carbonic anhydrase II (HCA II) is the fastest of at least 14 CA isozymes with a maximal turnover number of 10^6 s^{-1} (*13*, *14*). HCA II is a cytosolic enzyme consisting of a single polypeptide chain of 260 residues (*15*). The catalytic center of the spherically shaped enzyme resides at the bottom of a conical opening that is 15 Å in diameter at the mouth and 15 Å deep (*5*, *8*). At the base of the conical cleft resides a zinc atom that is tetrahedrally coordinated to three histidines (His94, His96, and His119) and a water/hydroxide ligand (Figure 1).

The catalysis of HCA II occurs in two distinctly separate steps referred to as ping−pong kinetics. The first step entails the nucleophilic attack of the Zn-bound (Zn-bound) hydroxide by the carbonyl carbon of CO_2, generating a bicarbonate ion. The second step involves the PT between the Zn-bound water and an exogenous buffer, thereby regenerating the initial Zn-bound hydroxide species (Figure 2) (*3*, *12*, *16*, *17*). The rate-limiting step of catalysis is dependent on the exogenous buffer concentration and is either the PT from His64 to the exogenous buffer at low buffer concentrations (*1*) or the PT from the Zn-bound water through the intramolecular water wire to His64 at high buffer concentrations (*18*). It has been suggested by both experiment and theory that the intramolecular water wire consists of 2−4 water molecules (*4*, *5*, *8*, *19*−*23*). These water molecules, which are believed to facilitate the transport of a proton 8−10 Å across the enzyme active site, are thought to be stabilized by Tyr7, Asn62, Asn67, Thr199, and Thr200 (Figure 1).

The importance of His64 has been illuminated by mutation experiments, where position 64 has been mutated to nonionizable residues such as alanine, which lead to a 10- to 50-fold reduction in the catalytic turnover, k_{cat}, for CO_2 hydration (*24*, *25*). Subsequent studies have chemically rescued these impaired mutants with 4-methyl-imidazole, recovering up to 40% of the maximal activity observed in the wild type (WT) system (*9*, *24*, *26*). These mutation and chemical rescue experiments suggest that His64 is intimately linked to the rate-limiting PT event in HCA II. X-ray data reveals that His64 adopts two orientations, labeled "in" or "out" (Figure 1) (*8*). It is not well understood how the orientation of His64 affects the rate-limiting PT event, if at all.

This work presents classical molecular dynamics (MD) simulations of the fully solvated HCA II enzyme, which were conducted to elucidate the role and behavior of His64 in

[†] This work was supported by the National Institute of Health (GM53148). The computational resources for this project have been provided by the National Institutes of Health (Grant number NCRR 1 S10 RR17214-01) on the Arches Metacluster, administered by the University of Utah Center for High Performance Computing.

* Corresponding author. Phone: (801) 581-7272. Fax: (801)581-4353. E-mail: voth@chem.utah.edu.

10.1021/bi062170f CCC: $37.00
Published on Web 02/24/2007

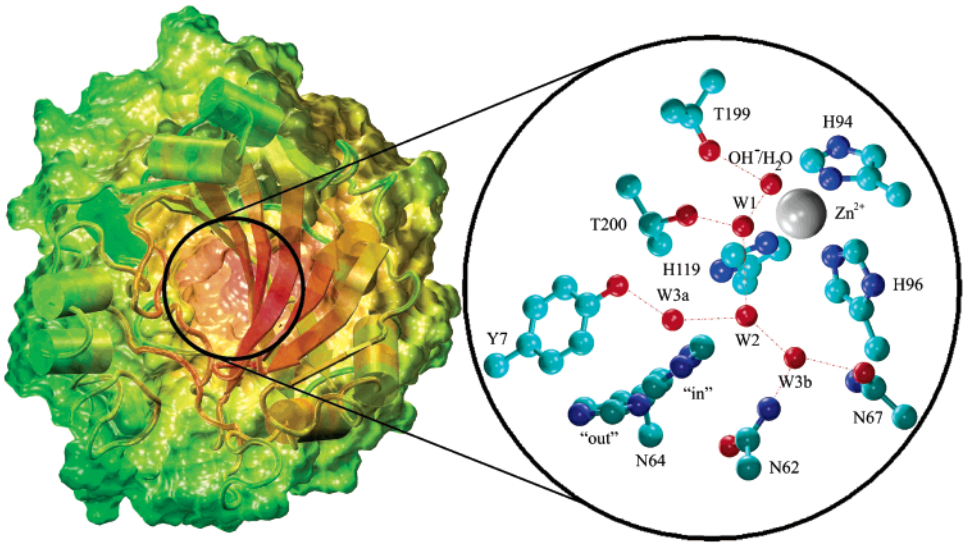

FIGURE 1: HCA II enzyme. This Figure depicts the solvent accessible surface of the HCA II enzyme. The color scale of the enzyme is based on the distance from the center of mass of the enzyme. The subset depicts the active site of HCA II from the 2CBA (*8*) X-ray crystallographic data where amino acids Tyr7, Asn62, Asn67, Thr199, and Thr200 are believed to stabilize the participating waters in the hydrogen-bonding network that links the Zn-bound water/hydroxide to His64 (*55*, *56*).

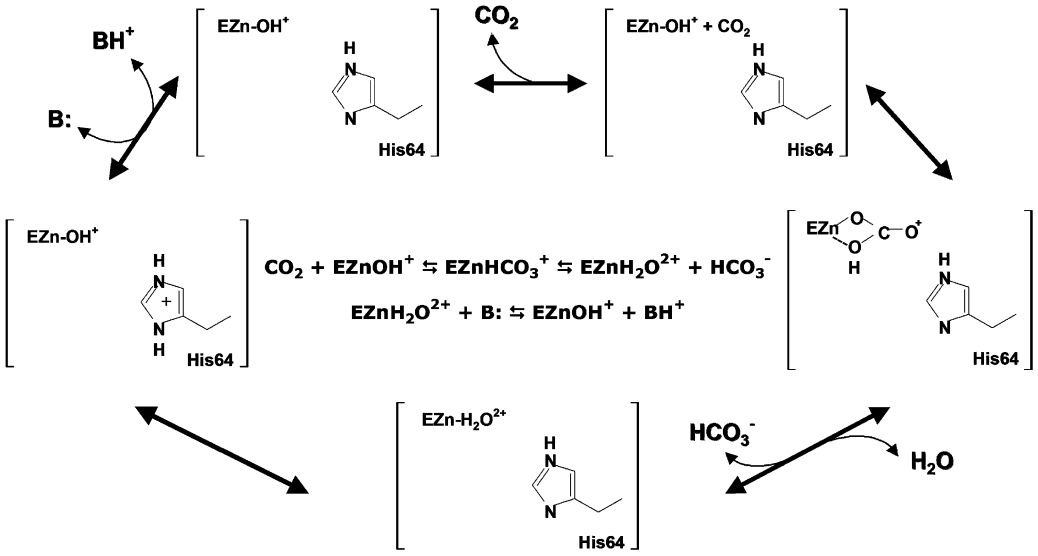

FIGURE 2: Catalytic mechanism of HCA II (*3*, *12*, *16*, *17*). The two end states studied are depicted in the bottom left two cells and are labeled EZn-H_2O^{2+} and EZn-OH^+. E stands for the enzyme HCA II, whereas Zn-H_2O^{2+} refers to the Zn-bound water and Zn-OH^+ refers to the Zn-bound hydroxide.

catalysis. Evaluation of two enzyme states was conducted to study the effects of the protonation state of His64 and the active site on the orientation of His64. These two states reflect the starting state in the hydration direction (Zn-bound water and a neutral His64) and the starting state in the dehydration direction (Zn-bound hydroxide and a protonated His64). In addition to studying different protonation states, the orientation of His64 was evaluated in both the "in" and "out" orientations. In the HCA II enzyme, an integral part of the catalysis is the formation of an intramolecular water wire that connects the catalytic zinc to His64. The ability of HCA II to form this critical water wire was evaluated for the two enzyme states and orientations of His64. In addition, key amino acids in the active site were analyzed for their ability to stabilize the intramolecular water wire. These analyses provide a more detailed picture of the orientation of His64 during the rate-limiting PT event at high buffer concentrations.

EXPERIMENTAL PROCEDURES

Four systems were created to represent the CO_2 hydration/dehydration reaction in HCA II. The initial state for the hydration reaction was modeled by a Zn-bound water and a neutral His64 (EZnH_2O^{2+}-His), whereas the initial state for the dehydration reaction was modeled by a Zn-bound hydroxide and a protonated His64 (E$ZnOH^+$-$HisH^+$). To evaluate the role of His64's orientation on the reaction, each of these initial systems were subdivided into two subsystems, defined by the orientation of the His64 residue. The starting configurations for the simulations were obtained from the 1.54 Å resolution X-ray structure (Protein Data Bank reference 2CBA) (*8*).

Partial Charges. To create a model that accurately represents a complex system, it is crucial to adequately describe the electrostatic interactions. For classical MD simulations, the electrostatic charge of an atom is represented

by a point charge centered on the nuclear coordinates. In complex systems, the environment in which an atom exists influences the charge density and subsequently the classical point charge counterpart. Therefore, a two-layered ONIOM (*27*−*35*) method in the Gaussian 03 (*36*) package was used to represent the HCA II system. The ONIOM method allows for a high-level electronic structure treatment on a small portion of the system without neglecting the effects of the overall system. This is crucial when dealing with enzymes, which use the total enzyme environment to catalyze a specific reaction. The two-layered ONIOM method consists of the total system and a small subset of the total system. The total system is treated with a low level of theory, whereas the small subset of the system is treated with both low and high levels of theory. The total ONIOM energy E^{ONIOM} is determined by the following equation (*28*, *29*)

$$E^{\mathrm{ONIOM}} = E(\mathrm{high},\mathrm{Model}_{\mathrm{subset}}) + E(\mathrm{low},\mathrm{Model}_{\mathrm{total}}) - E(\mathrm{low},\mathrm{Model}_{\mathrm{subset}}) \quad (2)$$

where $E(\mathrm{high},\mathrm{Model}_{\mathrm{subset}})$ is the energy of the small subset plus the link atoms calculated at the high level of theory, $E(\mathrm{low},\mathrm{Model}_{\mathrm{total}})$ is the energy of the total system at the low level of theory, and $E(\mathrm{low},\mathrm{Model}_{\mathrm{subset}})$ is the energy of the small subset at the low level of theory. The nuclear coordinates for the HCA II enzyme used in the ONIOM calculations were taken from equilibrated molecular dynamics (MD) structures (described below). The density functional method B3LYP (*37*, *38*) using the 6-31g(d) basis set was chosen as the high level of theory. The $\mathrm{Model}_{\mathrm{subset}}$ system consisted of His94, His96, His119, zinc, and the Zn-bound water/hydroxide (Figure 1). Hydrogen link atoms were used at the C_β site of the histidine backbone in order to fill exposed valence sites because of the truncation created at the ONIOM method boundary. The $\mathrm{Model}_{\mathrm{total}}$ system was represented using the AMBER parm96 (*39*) molecular mechanical (MM) force field. The MM parameters for the zinc active site were taken from previous MD simulation work (*20*, *40*). The $\mathrm{Model}_{\mathrm{total}}$ system consisted of the equilibrated HCA II enzyme and solvent water molecules within a 20 Å radius from the catalytic zinc atom. The embedded charges flag was used in the ONIOM method to allow the $\mathrm{Model}_{\mathrm{subset}}$ system to see the electrostatic charges of the $\mathrm{Model}_{\mathrm{total}}$ system. The ONIOM (B3LYP/6-31G(d):AMBER) system was optimized to find minima describing the $EZnH_2O^{2+}$-His and $EZnOH^{+}$-$HisH^{+}$ systems. Once the minima were obtained, charge calculations were performed at the Hartee−Fock level of theory using the 6-31g(d) basis set. The MM point charges were determined using the restrained electrostatic potential fitting procedure (*41*) (RESP) in the AMBER (*42*) package. Residual charges were added onto the C_β of the histidine backbones to force an integer charge on the systems.

MD Setup. The nuclear coordinates for the ONIOM RESP method calculations were taken from the first round of equilibration MD simulations on the HCA II system. The simulations represented the $EZnH_2O^{2+}$-His and the $EZnOH^{+}$-$HisH^{+}$ system, both having the His64 in the "in" orientation. The HCA II protein and 220 X-ray waters from the 2CBA-(*8*) X-ray structure were solvated in a cubic simulation box ($L \approx 75$ Å) of modified TIP3P (*43*) water. A total of 13,502 water molecules were added to the 4090 solute atoms for a total system size of 44,596 atoms. The parm99 (*44*) force field was used to describe the enzyme, whereas the parameters for the zinc active site were taken from Hoops et al. (*40*) and Lu and Voth (*20*, *40*). The modified parameters used to represent the active site are found in the Supporting Information. The first-round equilibration system was simulated for 250 ps in the constant NVE ensemble followed by 250 ps in the constant NPT ensemble (*45*). The resulting system was then equilibrated for 1ns in the constant NVT ensemble (*45*). All simulations were conducted at 298.15 K and used periodic boundary conditions with long-range Coulombic interactions calculated by the Ewald summation (*46*). The short-ranged nonbonded interactions and forces were subject to a 10 Å cutoff. The MD time integration step within the leapfrog Verlet integrator was 0.5 fs in all simulations. When applicable, the simulations were run at 1 atm and utilized Langevin dynamics for the thermostat. The simulations were carried out using the AMBER 8 package (*42*). The resulting geometries were then used as the initial geometries for the ONIOM RESP method calculations. The difference in Helmholtz free energy calculated in the current simulations is used interchangeably with differences in Gibbs free energy. This is accomplished because the system's average volume and pressure were constant with small fluctuations about the average values as seen from the equilibration period. In the approximation of constant volume and pressure with small fluctuations about the average, the differences in Gibbs and the differences in Helmholtz free energies may be directly compared.

Once new charges for the zinc active site were calculated for $(His)_3$-ZnH_2O^{2+} and $(His)_3$-$ZnOH^{+}$, they were implemented into the previously equilibrated systems (first-round equilibration). The parameters for the active site and the new RESP charges can be found in the Supporting Information. The newly modified systems were then subdivided into $EZnH_2O^{2+}$-His(IN/OUT) and $EZnOH^{+}$-$HisH^{+}$(IN/OUT). The "out" orientations were created by placing a harmonic restraint on the distance between the zinc and the N_δ of His64, $R_{\mathrm{Zn-N}_\delta}$, and using a spring force constant, k, of 40 kcal mol^{-1} $\mathrm{Å}^{-2}$. The four systems were then simulated for 250−500 ps in the constant NPT ensemble. The resulting systems were then subjected to another round of equilibration (second-round equilibration) that consisted of 1000 steps of steepest descent and 5000 steps of conjugated gradient optimization. The optimized system was then subjected to 200 ps of equilibration in the constant NPT ensemble and 2.5 ns in the constant NVT ensemble (*45*). All other simulation parameters were identical to the previously conducted first-round equilibration simulations.

Biased Sampling. Sampling a free energy surface that has characteristic features with significant barriers ($\gg k_B T$) is problematic for classical MD simulations. On such a free energy surface, a classical simulation will become trapped in a local minimum if such barriers surround it. To sample the full free energy surface, a biasing technique is required. With biased sampling, it is also necessary to use an unbiasing technique to combine the biased sample data to create a complete unbiased data set. The biasing umbrella sampling technique and the unbiasing weighted histogram analysis method (WHAM) (*47*, *48*) were used here to construct a potential of mean force (PMF) along the N-C_α-C_β-C_γ dihedral reaction coordinate, ξ_{dihedral}. This reaction coordinate de-

scribes the rotation of the imidazole group between the "in" and "out" orientation. Between 15 and 30 harmonic restraining potentials (windows) of the form

$$U_{\mathrm{n}}^{\mathrm{umbrella}}(\xi_{\mathrm{dihedral}}) = \frac{k_n}{2}(\xi_{\mathrm{dihedral}} - \xi_0^n)^2 \qquad (3)$$

were used to generate the PMF. All windows used spring constants of $k_n = 40$ kcal mol^{-1} rad^{-2} and spanned the range of $\xi_0^n = -65°$ to 80°. Each window was equilibrated for 250 ps followed by a data collection period of 1 to 2 ns in the constant NVT ensemble, depending on the convergence of the PMF. Convergence is considered achieved when there exists a negligible difference between a PMF calculated from the first half of the data and a PMF calculated from the second half of the data. In addition, the error of the PMF must be relatively small, ≤ 0.1 kcal/mol.

RESULTS AND DISCUSSION

Active Site Geometries. The second round of equilibration and subsequent umbrella sampling production runs for HCA II used the newly constructed RESP charges (Supporting Information) and modified parm99 (*44*) parameters (Supporting Information) (*20, 40*). In addition to these modified parameters, it was determined during the second round of equilibration that the distance between the zinc and the Zn-bound water was shorter than the X-ray and ONIOM values. This shortening of the bond was most likely due to the new charge distributions. To rectify the inaccurate bond length, a modification of the spring constant or equilibrium distance was needed. In the second round of equilibration and the umbrella sampling production runs, the equilibrium distance, r_{eq}, was increased to 2.30 Å, which yielded a zinc to Zn-bound water distance of 2.05 ± 0.09 Å. This value more closely reproduced the ONIOM results of 2.04 Å and is within the range of X-ray results of 1.99−2.08 Å, which were obtained over a range of pH values (*49*). The zinc to hydroxide and zinc to nitrogen (His94, His96 and His119) distances were not affected by the new charge distribution and resulted in good agreement with ONIOM and X-ray data.

His64 Orientation. When evaluating the orientation of amino acids containing ring structures, the χ_1 and χ_2 dihedral describes the spatial orientation of the side chain. The reaction coordinate (χ_1) involves the atoms N-C$_\alpha$-C$_\beta$-C$_\gamma$ and describes the rotation about the C$_\alpha$-C$_\beta$ atoms. This dihedral and the $R_{\mathrm{Zn-N}_\delta}$ distance are the primary factors in determining if the His64 residue is in the "in" or "out" orientation. The χ_2 dihedral contains the atoms C$_\alpha$-C$_\beta$-C$_\gamma$-N$_\delta$ and describes the rotation about the C$_\beta$-C$_\gamma$ atoms. The χ_2 dihedral determines the orientation of the imidazole ring of His64, which is often described as ring flipping. The free energy landscape as a function of χ_1 and/or χ_2 dictates the ability of the amino acid to sample its orientation space. The PMF for the rotation about the dihedral reaction coordinate, $F(\xi_{\chi 1})$ (Figure 3), provides information about the relative stability of His64 in either the "in" or "out" orientation as well as the free energy barrier, F_{b}, between the two orientations. The relative distributions of the "in" and "out" orientations from the $F(\xi_{\chi 1})$ can be compared to X-ray data and possibly help explain why some orientations are more prevalent in the X-ray structures. Evaluating both the χ_1 and χ_2 dihedrals along with the $R_{\mathrm{Zn-N}_\delta}$ distance will illuminate the spatial orientation of His64 in HCA II during the hydration/dehydration reaction. The F_{b} from the $F(\xi_{\chi 1})$ can be used with transition state theory to determine the upper limit for the rate of transfer between orientations, which can be compared to the rate-limiting step. This comparison of the rates helps determine if the movement between orientations is a factor in the rate-limiting step.

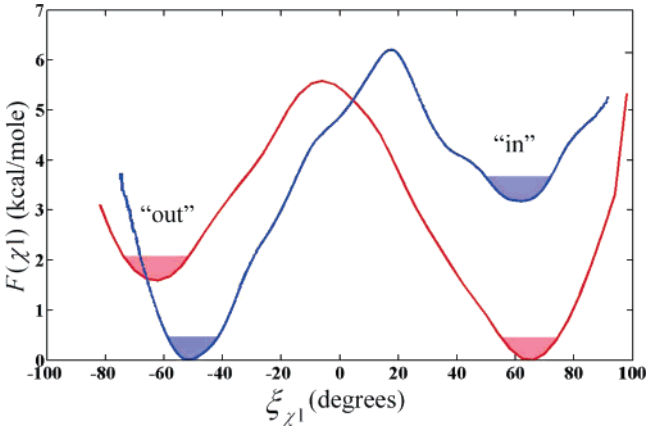

FIGURE 3: Free energy profile for rotation of His64 about the χ_1 dihedral angle in the EZn-H_2O^{2+}-His system (red) and the EZn-OH^+-$HisH^+$ system (blue). Error for the PMFs is less than 0.1 kcal/mol as determined by Monte Carlo bootstrap error analysis. The filled portion of the wells represents the thermally accessible region of the dihedral within $k_{\mathrm{B}}T/2$ of the minimum.

The PMFs, $F(\xi_{\chi 1})$, for the EZnH_2O^{2+}-His and the EZnOH^+-$HisH^+$ systems are displayed in Figure 3. For His64 in the EZnH_2O^{2+}-His system, the "in" orientation is described by the dihedral angles of $-7° \leq \chi_1 \leq 100°$, whereas the "out" orientation is described by the dihedral angles of $-100° \leq \chi_1 \leq -7°$, where the transition state region is around −7.0°. The F_{b} for rotation about the χ_1 dihedral from "in" to "out" is 5.6 kcal mol^{-1} with the "in" orientation being 1.6 kcal mol^{-1} more stable. By contrast, the EZnOH^+-$HisH^+$ system's "in" orientation is described by the dihedral angles of $17° \leq \chi_1 \leq 100°$, and the "out" orientation is described by the dihedral angles of $-100° \leq \chi_1 \leq 17°$, where the transition state region is located near 17°. The F_{b} for rotation about the χ_1 dihedral from "out" to "in" is 6.2 kcal mol^{-1} with the "out" orientation being 3.2 kcal mol^{-1} more stable. The $F(\xi_{\chi 1})$ free energy curve for the EZnOH^+-$HisH^+$ system not only has a higher F_{b} but also has a stability of the "in" to "out" orientation that is opposite that for the EZnH_2O^{2+}-His system. This suggests that the orientation of His64 may be susceptible to long-range electrostatic interactions with the active site and differing solvent environments for the two systems.

The rate at which His64 traverses from the "in" to the "out" orientation is important in determining if this rotation plays a role in the rate-limiting step of catalysis. The rate of transversal is also crucial in determining if the orientation of His64 has time to reach equilibrium on the time scale of the rate-limiting PT event. Transition state theory provides an approximate bridge between the F_{b} and the rate of transmission over the barrier by virtue of the following formula

$$k_{\mathrm{TST}} = \frac{\omega_0}{2\pi} e^{(-F_{\mathrm{b}}/k_{\mathrm{B}}T)} \qquad (4)$$

where k_{TST} is the rate of transmission in the approximation of the TST limit, $\beta = (1/k_BT)$, where k_B is Boltzmann's constant, T is the temperature, ω_0 is the fundamental frequency of the reactant state around its minimum, and F_b is the free energy barrier height. The fundamental frequency, ω_0, was calculated using normal-mode analysis conducted on a subsystem of the HCA II enzyme. The first system consisted of residues 5, 6, 7, 63, 64, and 65, whereas the second system consisted of residues 3−8, 61−67, and 197−201. The coordinates for the normal mode systems were taken from the average structure of the 2.5 ns trajectory of the HCA II enzyme with His64 in the "in" orientation. The α-carbons of all residues except 64 were constrained to their average positions, and the system was then optimized using the steepest decent method. The optimized structure was then treated by normal-mode analysis using the parm99 force field. The resulting frequencies were then analyzed for ω_0. Both the small and larger systems produced similar ω_0 values of 159.59 and 161.68 cm^{-1}, respectively. By then using eq 4, it was found that the "out" to "in" transition for the $EZnH_2O^{2+}$-His system is over 1 order of magnitude faster than the "in" to "out" transition and 3 orders of magnitude faster than the hydration PT rate of native HCA II (*50*). Conversely, in the $EZnOH^+$-$HisH^+$ system, the "in" to "out" transmission is 2 orders of magnitude greater than the "out" to "in" transmission and 4 orders of magnitude greater than the PT rate of native HCA II. This rate information suggests that the rotation of His64 about the χ_1 dihedral has ample time to reach equilibrium between PT events in HCA II for both the $EZnH_2O^{2+}$-His and $EZnOH^+$-$HisH^+$ systems. Therefore, using the equilibrium distribution from the $F(\xi_{\chi 1})$ curves becomes valid in analyzing the orientation of His64 in HCA II on the time scale of the rate-limiting PT event. Because the transmission rates are significantly faster than the rate-limiting step of HCA II, we can rule out these transmissions of His64 as a direct factor in the rate-limiting step.

An inspection of the $F(\xi_{\chi 1})$ curves also reveals a shifting of the transition state (TS) from $\chi_1 = -7°$ in $EZnH_2O^{2+}$-His to $\chi_1 = 17°$ in the $EZnOH^+$-$HisH^+$ system. To understand the cause of the χ_1 dihedral shift, the relationship between the χ_1 dihedral and the distance between the catalytic zinc and the N_δ of His64 (R_{Zn-N_δ}) was evaluated (Figure 4). From Figure 4, it is apparent that the shift in the χ_1 dihedral corresponds to an increase in R_{Zn-N_δ} of around 2 Å. The increase in R_{Zn-N_δ} is most likely due to the repulsive nature of two positively charged bodies (active site and His64). The "in" and "out" orientations previously defined by the χ_1 dihedral can also be defined by R_{Zn-N_δ}, with the "in" orientation corresponding to R_{Zn-N_δ} of around 7 Å and the "out" orientation corresponding to distances around 11 Å. Evaluating R_{Zn-N_δ} as a function of χ_1 indicates that His64 prefers to occupy very specific distances from the catalytic zinc over a range of χ_1 (Figure 4). For the $EZnH_2O^{2+}$-His system, R_{Zn-N_δ} distances stay relatively stable at 11.5 Å, until the χ_1 approaches the TS at −7°, at which point the R_{Zn-N_δ} distance, after passing through the TS region, changes to values around 7.5 Å. The majority of the R_{Zn-N_δ} change occurs in the range of $-20° \leq \chi_1 \leq 10°$ and again at $25° \leq \chi_1 \leq 35°$. Figure 4 shows that in the region where R_{Zn-N_δ} distances are typical of the "in" orientation, the dihedral samples a range of $-70° \leq \chi_1 \leq -20°$, whereas the dihedral samples $35° \leq \chi_1 \leq 90°$ when in the "out" orientation. An

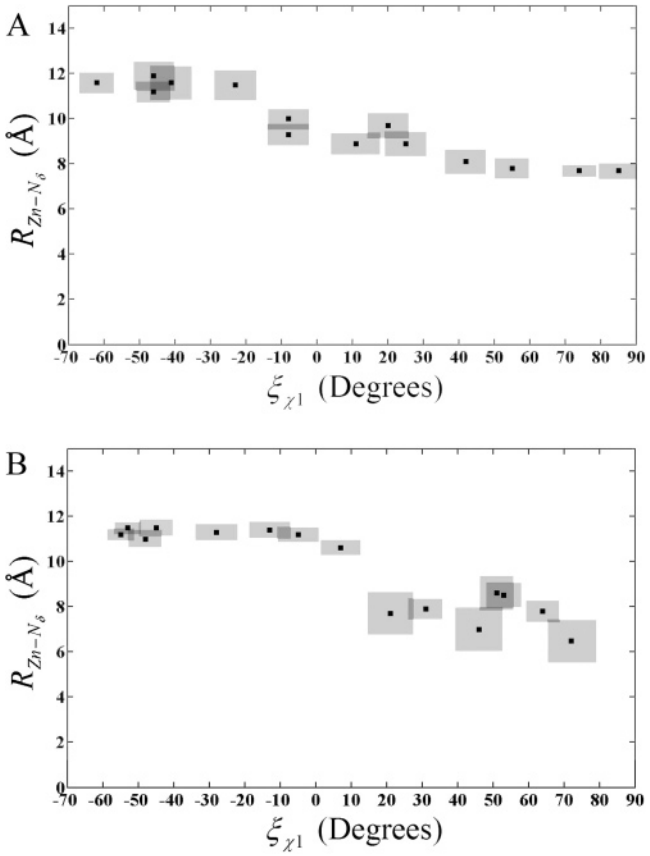

FIGURE 4: Distance from catalytic zinc to the N_δ of His64 as a function of the χ_1 dihedrals for the $EZn\text{-}H_2O^{2+}$-His system (A) and the $EZn\text{-}OH^+$-$HisH^+$ system (B). The solid black squares represent the average $R_{Zn-N_\delta}(\chi_1)$ value. The shaded area around the solid squares represents the uncertainty in the calculated R_{Zn-N_δ} and the χ_1 values.

inspection of the R_{Zn-N_δ} distances reveals an abrupt change at the TS, which indicates that the $EZnH_2O^{2+}$-His system prefers to have His64 at very specific distances that may correspond to environments that favor PT. Given that 7.5 Å is indicative of the "in" orientation, three to four water molecules would be needed to bridge the span between the catalytic zinc and His64. Indeed, water wires containing three or four water molecules are seen in both MD simulation data (data not shown) and X-ray data (*51*). When His64 occupies the "out" orientation, the increased R_{Zn-N_δ} allows for the addition of one or more water molecules to the water wire, as seen in MD simulation data (data not shown). The discrete R_{Zn-N_δ} distances seen as the χ_1 angle varies could be partially explained by the sequential insertion/deletion of water molecules from the water wire. The $EZnOH^+$-$HisH^+$ system also possesses this discrete distance characteristic for $R_{Zn-N_\delta}(\chi_1)$. For the $EZnOH^+$-$HisH^+$ system, a stable R_{Zn-N_δ} region of 11 to 12 Å across the range of $-60° \leq \chi_1 \leq 0°$ is representative of the "out" orientation. Near the TS, the N_δ of His64 abruptly moves to the "in" orientation with a R_{Zn-N_δ} of 7 to 8 Å. A distinct difference between the $EZnH_2O^{2+}$-His system and the $EZnOH^+$-$HisH^+$ system is the wider transition region in the $EZnH_2O^{2+}$-His system. The wider transition region is expected because of the broad transition region in the $EZnH_2O^{2+}$-His system's PMF when compared to that of the $EZnOH^+$-$HisH^+$ system (Figure 3).

To see the spatial orientation of the His64 more clearly, it is useful to evaluate the PMF as a function of χ_1 as well

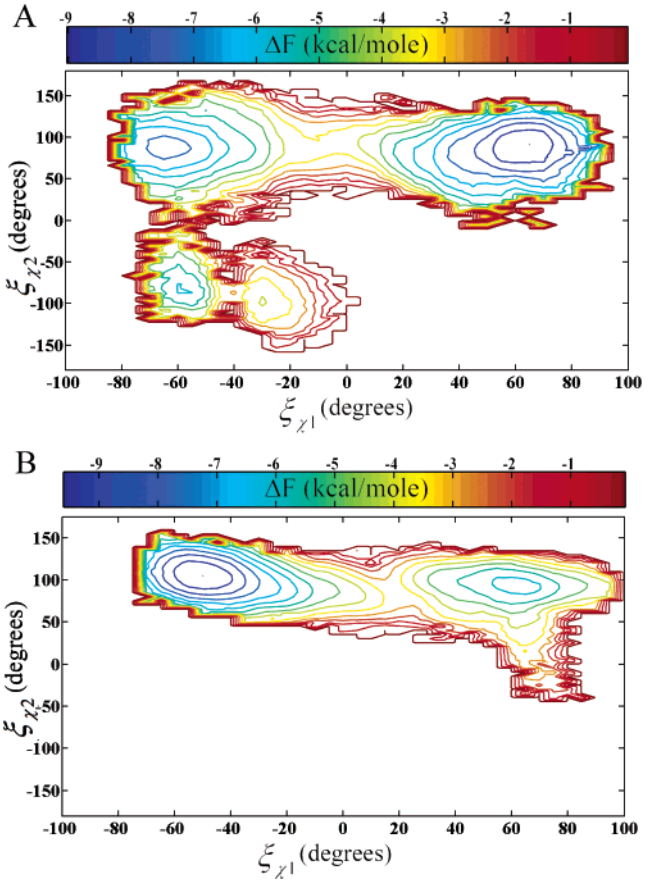

FIGURE 5: Free energy profile for the rotation about the dihedral angles as a function of χ_1 and χ_2. (A) $F(\xi_{\chi 1},\xi_{\chi 2})$ for the $EZnH_2O^{2+}$-His system. (B) $F(\xi_{\chi 1},\xi_{\chi 2})$ for the $EZnOH^+$-$HisH^+$ system.

as χ_2 (Figure 5). The two-dimensional (2-D) PMF, $F(\xi_{\chi 1},\xi_{\chi 2})$, can be constructed using the following equation (*52*)

$$F(\xi_{\chi 1},\xi_{\chi 2}) = F(\xi_{\chi 1}) - k_B T \ln\langle\rho(\xi_{\chi 2};\xi_{\chi 1})\rangle + C \quad (5)$$

where $F(\xi_{\chi 1})$ is the free energy as a function of $\xi_{\chi 1}$, $\langle\rho(\xi_{\chi 2};\xi_{\chi 1})\rangle$ is the average density along $\xi_{\chi 2}$ at a given $\xi_{\chi 1}$, and C is a constant. When evaluating the 2-D PMF for the $EZnH_2O^{2+}$-His system, the χ_2 dihedral transverses the range of $4° \leq \chi_2 \leq 140°$ when the χ_1 dihedral is in the range depicting the "in" orientation and transverses the range of $-148° \leq \chi_2 \leq 156°$ when the χ_1 dihedral is in the range depicting the "out" orientation. When His64 is inserted into the active site, "in" orientation, the imidazole ring adopts two stable orientations. The two orientations are the "parallel" orientation for dihedrals of $\sim 20° \leq \chi_2 \leq \sim 100°$ and the "perpendicular" orientation for dihedrals of $\sim 100° \leq \chi_2 \leq \sim 150°$. The orientation of His64 with respect to the catalytic zinc is shown in Figure 6. Figure 5A reveals a free energy barrier between the two local minima describing the parallel and perpendicular orientation of His64, indicating that the χ_2 dihedral between these two local minima is infrequently sampled. From the 2-D PMF, the barrier for ring flipping, χ_2, is around 7 kcal/mol, which is in close agreement with the proposal that ring flipping about the side chains χ_2 dihedral has a barrier of ≤ 8 kcal/mol corresponding to rates of $\geq 10^6$ s^{-1} (*53*). When His64 adopts the "out" orientation, there are less restrictions on the rotation of the imidazole ring as seen by the larger sampling of the χ_2 dihedral, Figure 5A. In the "out" orientation, the imidazole ring of His64 rotates from having the N_δ facing the catalytic zinc (parallel) to having the imidazole ring occupying two different perpendicular orientations. This increased ability for rotation could be explained by the fact that the His64's environment is less restrictive in the "out" orientation due to the His64 occupying a more bulk water-like environment.

The χ_1 and χ_2 2-D PMF for the $EZnOH^+$-$HisH^+$ system is depicted in Figure 5B. The overall χ_2 range is smaller than that of the $EZnH_2O^{2+}$-His system (Figure 6). When χ_1 is in the "in" orientation, the χ_2 dihedral samples from $\sim -40° \leq \chi_2 \leq \sim 150°$ with $\sim -40° \leq \chi_2 \leq \sim 100°$ represented by the parallel orientation and $\sim 100° \leq \chi_2 \leq \sim 150°$ representing the perpendicular orientation. One significant difference between the $EZnH_2O^{2+}$-His system and the $EZnOH^+$-$HisH^+$ system is the increased χ_2 sampling for the $EZnOH^+$-$HisH^+$ system in the "in" orientation. This can be explained by the almost symmetric charge distribution on $HisH^+$. This in turn supports the idea that the N_δ and N_ϵ of the $HisH^+$ moiety are almost indistinguishable in the active site environment, allowing $HisH^+$ of the $EZnOH^+$-$HisH^+$ system to rotate to either perpendicular orientation. This is not the case for the His moiety in the $EZnH_2O^{2+}$-His system because the N_δ and N_ϵ are significantly different, and therefore, only one perpendicular orientation is sampled. When χ_1 is in the "out" orientation, the χ_2 for the $EZnOH^+$-$HisH^+$ system samples a reduced range of $\sim 50° \leq \chi_2 \leq \sim 150°$, which includes one of the two perpendicular orientations and the parallel orientation. Only one perpendicular orientation is sampled because the ring structure of Trp5 interacts with the positively charged imidazolium ring of His64, thereby restricting the rotation of His64. Even though Trp5 is present in both the $EZnH_2O^{2+}$-His and the $EZnOH^+$-$HisH^+$ systems, the extra proton of the $HisH^+$ moiety now prevents certain rotations of the His64 ring near Trp5.

An important aspect of the free energy curve, $F(\xi)$, is the ability to calculate the equilibrium probability of finding His64 in either the "in" or "out" orientation, which can then be compared to experimental X-ray data. The relative distribution of the "in" to "out" orientation is found by integrating the PMF curve according to the following equation

$$P = \frac{\int_a^b e^{-\beta F(\xi)} d\xi}{\int_{-180}^{180} e^{-\beta F(\xi)} d\xi} \quad (6)$$

where P is the probability, ξ is the reaction coordinate, a and b represent the subset range of configurations, and $F(\xi)$ is the free energy. Typically, the ranges for integration are $-180° \leq a \leq$ TS and TS $\leq b \leq 180°$. Using eq 6 yields an "in" orientation probability of 86.2% and an "out" orientation probability of 13.8% for the $EZnH_2O^{2+}$-His system and a probability of 3.3% for the "in" orientation and 96.7% for the "out" orientation in the $EZnOH^+$-$HisH^+$ system. The appearance of both the "in" and "out" orientations is also seen in X-ray data where both the "in" and "out" orientations are present at different ratios over the pH range of 6.1−10 (*2*, *49*). The ratio values for the $EZnH_2O^{2+}$-His system agree very well with recent X-ray data that indicates a ratio of 80% "in" and 20% "out" (*51*). This agreement would also indicate that the X-ray structure is representative of the $EZnH_2O^{2+}$-His system and not the $EZnOH^+$-$HisH^+$ system.

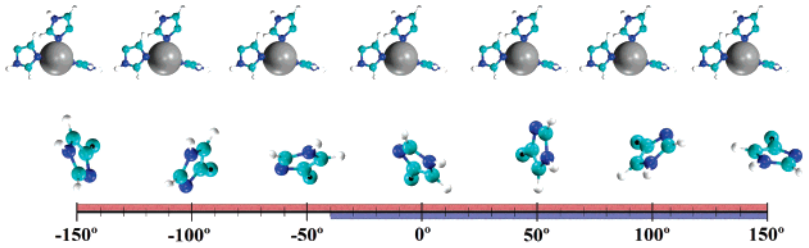

FIGURE 6: Orientation of His64 with respect to the catalytic zinc as a function of the χ_2 dihedral. The black dot indicates the C_β of the His64 backbone. The red line represents the range of the χ_2 dihedral angles sampled for the $EZnH_2O^{2+}$-His system, whereas the blue line represents the range of the χ_2 dihedral angles sampled for the $EZnOH^+$-$HisH^+$ system (*55*, *56*).

Analyzing the $F(\xi)$ value reveals that when His64 is protonated, like in the $EZnOH^+$-$HisH^+$ system, it predominantly adopts the "out" orientation while adopting the "in" orientation for the $EZnH_2O^{2+}$-His system. This suggests that when HCA II proceeds in the CO_2 hydration direction ($EZnH_2O^{2+}$-His as reactant), the His64 is in the "in" orientation. This moves the N_δ of His64 closer to the catalytic zinc and maximizes the probability of PT from the Zn-bound water to His64. Whereas in the $EZnOH^+$-$HisH^+$ system where His64 prefers the "out" orientation, the PT from His64 to the bulk medium is favored over the PT from His64 to the catalytic Zn-bound hydroxide.

His64 Solvation Structure. The solvent structure around His64 should be crucial in the transport of a proton near the imidazole ring. It is the water solvent that is believed to transport the proton between the catalytic active site and His64. The solvent is also responsible for the transport of the proton between the bulk water environment and His64. Therefore, 2-D radial distribution functions (RDF) were calculated on the HCA II simulations to evaluate how the solvent network adapts to the orientation of His64. The 2-D RDF around the N_δ of His64 at different χ_1 dihedrals, $g(\xi_{\chi1}, \xi_{R_{N_\delta-OW}})$, was evaluated to clarify the behavior of the solvation shells for both the ZnH_2O^{2+}-His and $ZnOH^+$-$HisH^+$ systems (Figure 7). It has been shown that the RDF for the modified TIP3P reasonably reproduces the experimentally determined RDFs for bulk water (data not shown). When His64 adopts the "in" orientation in the ZnH_2O^{2+}-His system, the second solvation shell's amplitude is slightly elevated above that of the first solvation shell. Closer inspection of the first solvation shell reveals an average occupancy of 1.1 (data not shown). The W3a (Figure 1) water is clearly the major contributor of the peak's amplitude with a minor portion being contributed by either W2 or another active site water. Because of the stabilizing hydrogen bonds and the reduced volume in the active site, the W3a water is believed to be the predominant water in the vicinity of the N_δ of His64. The W2 and other active site waters predominantly occupy the second solvation shell. The second solvation shell has a relatively elevated amplitude because these enzyme-stabilized waters have a reduced diffusion constant compared to that of bulk water (*19*) and occupy this solvation shell.

The small amplitude in $g(\xi_{\chi1},\xi_{R_{N_\delta-OW}})$ in Figure 7 at around 10 Å can be explained by the solution void created by the HCA II enzyme. As the His64 retracts from the confined active site of the enzyme and starts to experience a more bulk-like solvated environment, the amplitude of the second solvation shell decreases. This reduction in the second solvation shell's amplitude is due to more labile waters occupying the second solvation shell, typical of a more bulk

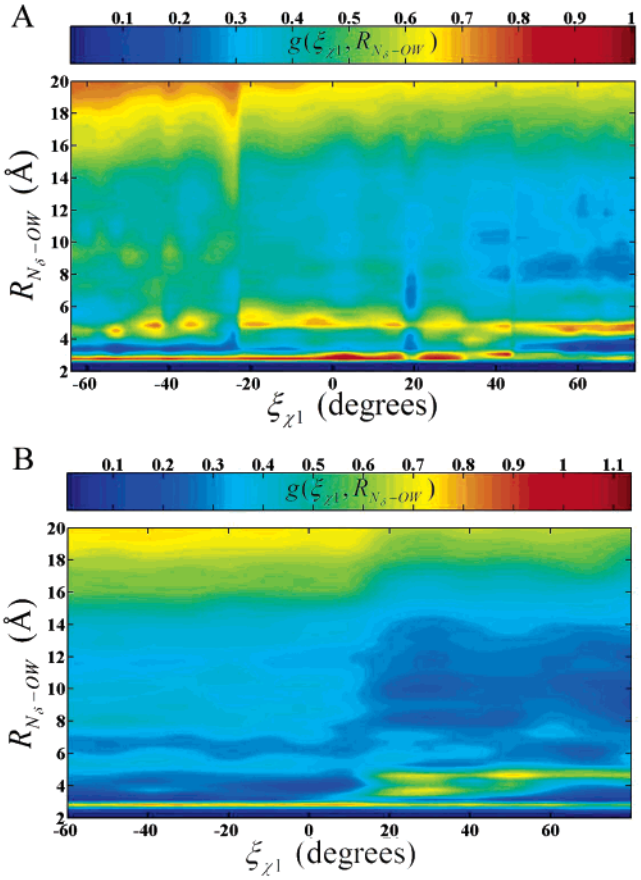

FIGURE 7: 2-D radial distribution function. (A) $g(\xi_{\chi1},R_{N_\delta-OW})$ for the $EZnH_2O^{2+}$-His system. (B) $g(\xi_{\chi1},R_{N_\delta-OW})$ for the $EZnOH^+$-$HisH^+$ system.

water like environment. In addition, the first solvation peak increases slightly because His64 is removed from the solvent network in the enzyme environment, and more waters are allowed to favorably interact with the first solvation shell. As the His64 moves to the "out" orientation, the elevated first solvation amplitude persists, and the second solvation shells amplitude is reduced. The "out" orientation reflects a more classical bulk-like RDF for histidine, with the major difference being that the bulk density values of the $g(\xi_{\chi1}, \xi_{R_{N_\delta-OW}})$ do not become apparent until $R_{N_\delta-OW} > 18$ Å in the enzyme system, where one would expect a histidine in bulk water to reach bulk density at a shorter distance (~6 Å). Again, this is explained by the solvation void created by the HCA II enzyme, which suppresses the amplitude of the radial distribution function because no water is present in the enzyme void.

The 2-D RDF for the $EZnOH^+$-$HisH^+$ system in Figure 7B, like the $EZnH_2O^{2+}$-His system, shows significant

changes in the solvation structure at different χ_1 dihedrals. When His64 is in the "in" orientation, there are two prominent solvation shells followed by the void at around 10 Å. Once again, it is evident that the second solvation shell has an elevated amplitude because of the stabilizing effect of the active site amino acids on the active site waters. The second solvation shell is also at a shorter $R_{N_\delta-OW}$ than that seen in bulk water. This is an indication of the level of frustration in the solvent environment. Frustration in this case refers to the amount by which the solvation structure must deviate from bulk values in order to accommodate a particular environment. It can be concluded that $HisH^+$ occupies a more frustrated environment in the "in" orientation than His because His deviates from the bulk-like RDF in amplitude only, whereas $HisH^+$ deviates from the bulk-like RDF in amplitude and spacing. This frustration is postulated as one of the reasons the "in" orientation is less favorable for $HisH^+$. As the χ_1 dihedral is reduced and the His64 begins to move to the "out" orientation, a transition phase is seen in the behavior of $g(\xi_{\chi 1},\xi_{R_{N_\delta-OW}})$. The transition state at $\chi_1 = 17°$ is evident in the $g(\xi_{\chi 1},\xi_{R_{N_\delta-OW}})$ by the termination of the second solvation shell at around 4 Å. As His64 moves to the "out" orientation, the first solvation shell intensity increases, the second and third solvation shells move to longer $R_{N_\delta-OW}$ distances, and a noticeable void forms before and after the second solvation shell. This indicates that $HisH^+$ is able to form an ordered and stable solvation structure when in the "out" orientation. The solvation structure is more ordered in $EZnOH^+$-$HisH^+$ than in the $EZnH_2O^{2+}$-His system because the $EZnOH^+$-$HisH^+$ system's His64 carries a positive charge and, therefore, creates more electrostatic interactions. The "out" orientation's behavior of $g(\xi_{\chi 1},\xi_{R_{N_\delta-OW}})$ is very similar to that of $HisH^+$ in bulk water except for the shifted tail region at longer $R_{N_\delta-OW}$ distances. Again, the bulk density value is not reached until greater $R_{N_\delta-OW}$ values because of the presence of the HCA II enzyme.

CONCLUSIONS

The present investigation into the orientation of His64 in HCA II has revealed a complex interplay between His64 and its environment. PMF data along the reaction coordinate, χ_1, reveals the long-range electrostatic interactions between His64, the solvent environment, and the active site of HCA II. In the HCA II system, transition state theory suggests that on the time scale of the rate-limiting PT event, the transfer between orientations for His64 does not contribute to the rate-limiting step, and His64 will have reached equilibrium between the "in" and "out" orientations. Once in equilibrium, the His64 of $EZnH_2O^{2+}$-His system is favored to occupy the "in" over the "out" orientation. This indicates that His64 favorably inserts into the active site, thereby decreasing the distance between the catalytic zinc and N_δ of His64. This shortened distance between the catalytic zinc and His requires shorter water wires to connect the Zn-bound water to the N_δ of His64, which are believed to be more conducive to PT.

In the $EZnOH^+$-$HisH^+$ system, the PMF data suggests that the "out" orientation is favored at equilibrium over the "in" orientation. The protonated His64 for the $EZnOH^+$-$HisH^+$ system is more likely to rotate to the "out" orientation and release the proton to the bulk water than to remain in the "in" orientation and back-donate the proton to the Zn-bound hydroxide. This step appears to be a key feature of the overall enzyme functional cycle.

In addition to the χ_1 dihedral effects reflecting the "in" versus "out" conformation, the $\chi 2$ dihedral, which describes the imidazole ring orientation, plays a role in the ability for His64 to find a favorable orientation relative to the enzyme active site. The His for the $EZnH_2O^{2+}$-His system is restricted in its sampling of the χ_2 dihedral when χ_1 is in the "in" orientation because of the elevated χ_2 barrier when compared to the $EZnOH^+$-$HisH^+$ system. The barrier height and subsequently the sampling of the χ_2 dihedral causes an increase in the probability that His will be in the optimum orientation for PT from the Zn-bound water to His64. At the same time, the reduced χ_2 barrier (Figure 5) and, therefore, the increased sampling of χ_2 in the "in" orientation for the $EZnOH^+$-$HisH^+$ system reduces the probability that $HisH^+$ will occupy the ideal conformation for PT to the Zn-bound hydroxide. This intricate interplay between χ_1 and χ_2 dihedrals reveals how the enzyme environment manipulates His64 to occupy the most favorable position for catalysis in HCA II. In future work, the present results will be integrated with those from the simulations of explicit PT using the multi-state empirical valence bond (MS-EVB) model (*54*) as applied to HCA.

SUPPORTING INFORMATION AVAILABLE

Detailed information on the modifications to the force field. This material is available free of charge via the Internet at http://pubs.acs.org.

REFERENCES

1. Lindskog, S., Behravean, G., Engstrand, C., Forsman, C., Jonsson, B., Liang, Z., Ren, X., and Xue, Y. (1991) in *Carbonic Anhydrase-From Biochemistry and Genetics to Physiology and Clinical Medicine* (Botre, F., Gros, G., Storey, B. T., Ed.) pp 1−13, VCH, Weinheim, Germany.
2. Nair, S. K., and Christianson, D. W. (1991) Unexpected pH-dependent conformation of His-64, the proton shuttle of carbonic anhydrase II, *J. Am. Chem. Soc. 117*, 9455−9458.
3. Christianson, D. W. (1991) The structural biology of zinc, *Adv. Protein Chem. 42*, 281−355.
4. Lesburg, C. A., and Christianson, D. W. (1995) X-ray crystallographic studies of engineered hydrogen bond networks in protein zinc binding site, *J. Am. Chem. Soc. 117*, 6838−6844.
5. Eriksson, A. E., Jones, A. T., and Liljas, A. (1988) Refined structure of human carbonic anhydrase II at 2.0 Å resolution, *Proteins 4*, 274−282.
6. Liljas, A., Kannan, K. K., Bergsten, P. C., and Waara, I. (1972) Crystal structure of human carbonic anhydrase C, *Nature 235*, 131−137.
7. Kannan, K. K., Ramanadham, M., and Jones, T. A. (1984) Structure, refinement, and function of carbonic anhydrase I, *Ann. N.Y. Acad. Sci. 429*, 49−60.
8. Håkansson, K., Carlsson, M., Svensson, L. A., and Liljas, A. (1992) Structure of native and apo carbonic anhydrase II and structure of some of its anion-ligand complexes, *J. Mol. Biol. 227*, 1192−1204.
9. Duda, D., Tu, C., Qian, M., Laipis, P., Agvandje-McKenna, A., Silverman, D. N., and McKenna, R. (2001) Structural and kinetic analysis of the chemical rescue of the proton transfer function of carbonic anhydrase II, *Biochemistry 40*, 1741−1748.
10. Duda, D., Govindasamy, L., Agbandje-McKenna, Tu, C., Silverman, D. N., and McKenna, R. (2003) The refined atomic structure of carbonic anhydrase II at 1.05 Å resolution: implications of chemical rescue of proton transfer, *Acta Crystallogr., Sect. D 59*, 93−104.

11. Fersnt, A. (1985) *Enzyme Structure and Mechanism*, W. H. Freeman, New York.
12. Silverman, D. N., and Lindskog, S. (1988) The catalytic mechanism of carbonic anhydrase: implications of a rate-limiting protolysis of water, *Acc. Chem. Res. 21*, 30−36.
13. Maren, T. H. (1967) Carbonic anhydrase: chemistry, physiology, and inhibition, *Physiol. Rev. 47*, 595−781.
14. Tashian, R. E. (1989) The carbonic anhydrase: widening perspectives on their evolution, expression and function, *BioEssays 10*, 186−192.
15. Henderson, L. E., Hendriksson, D., and Nyman, P. O. (1976) Primary structure of human carbonic anhydrase, *J. Biol. Chem. 251*, 5457−5463.
16. Lindskog, S., and Coleman, J. E. (1973) The catalytic mechanism of carbonic anhydrase, *Proc. Natl. Acad. Sci. U.S.A. 70*, 2505−2508.
17. Lindskog, S. (1983) In *Zinc Enzymes* (Spiro, I. G., Eds.) pp 78−121, John Wiley & Sons, New York.
18. Silverman, D. N., and Vincent, S. H. (1983) Proton transfer in the catalytic mechanism of carbonic anhydrase, *CRC Crit. Rev. Biochem. 14*, 207−255.
19. Toba, S., Colombo, G., and Merz, K. M., Jr. (1999) Solvent dynamics and mechanism of proton transfer in human carbonic anhydrase II, *J. Am. Chem. Soc. 121*, 2290−2302.
20. Lu, D., and Voth, G. A. (1998) Molecular dynamics simulations of human carbonic anhydrase II: insights into experimental results and the role of solvation, *Proteins: Struct., Funct., Genet. 33*, 119−134.
21. Lu, D., and Voth, G. A. (1998) Proton transfer in the enzyme carbonic anhydrase: an *ab initio* study, *J. Am. Chem. Soc. 120*, 4006−4014.
22. Cui, Q., and Karplus, K. (2003) Is a "proton wire" concerted or stepwise? A model study of proton transfer in carbonic anhydrase, *J. Phys. Chem. B 107*, 1071−1078.
23. Riccardi, D., Schaefer, P., Yang, Y., Yu, H., Ghosh, N., Prat-Resina, X., Konig, P., Li, G., Xu, D., Guo, H., Elstner, M., and Cui, Q. (2006) Development of effective quantum mechanical/molecular mechanical (QM/MM) methods for complex biological processes, *J. Phys. Chem. B 110*, 6458−6469.
24. Tu, C., Silverman, D. N., Forsman, C., Jonsson, B.-H., and Lindskog, S. (1989) Role of histidine 64 in the catalytic mechanism of human carbonic anhydrase II studied with a stie-specific mutant, *Biochemistry 28*, 7913−7918.
25. Qian, M., Tu, C., Earnhardt, N., Laipis, P. J., and Silverman, D. N. (1997) Gultamate and aspartate as proton shuttles in mutants of carbonic anhydrase, *Biochemistry 36*, 15758−15764.
26. An, H., Tu, C., Duda, D., Montanez-Clemente, I., Math, K., Laipis, P. J., McKenna, R., and Silverman, D. N. (2002) Chemical rescue in catalysis by human carbonic anhydrase II, *Biochemistry 41*, 3235−3242.
27. Dapprich, S., Komaromi, I., Byun, K. S., Morokuma, K., and Frisch, M. J. (1999) A new ONIOM implementation in Gaussian98. Part I. The calculation of energies, gradients, vibrational frequencies and electric field derivatives. *J. Mol. Struct. 462*, 1−21.
28. Humbel, S., Sieber, S., and Morokuma, K. (1996) The IMOMO method: Integration of different levels of molecular orbital approximations for geometry optimization of large systems: Test for n-butane conformation and SN2 reaction: RCL + Cl^-, *J. Chem. Phys. 105*, 1959−1967.
29. Kuno, M., Hannongbua, S., and Morokuma, K. (2003) Theoretical investigation on nevirapine and HIV-1 reverse transcriptase binding site interaction based on ONIOM method, *Chem. Phys. Lett. 380*, 456−463.
30. Maseras, F., and Morokuma, K. (1995) IMOMM: A new ab initio + molecular mechanics geometry optimization scheme of equilibrium structures and transition states, *J. Comput. Chem. 16*, 1170−1179.
31. Svensson, M., Humbel, S., Froese, R. D. J., Matsubara, T., Sieber, S., and Morkima, K. (1996) ONIOM: A multilayered integrated MO + MM method for geometry optimizations and single point energy predictions. A test for Diels-Alder reactions and Pt(P(t-Bu)3)2 + H2 oxidative addition, *J. Phys. Chem. 100*, 19357−19363.
32. Svensson, M., Humbel, S., and Morkuma, K. (1996) Energetics using the single point IMOMO (integrated molecular orbital + molecular orbital) calculations. Choices of computational levels and model system, *J. Chem. Phys. 105*, 3654−3661.
33. Vreven, T., and Morokuma, K. (2000) On the application of the IMOMO (integrated molecular orbital + molecular orbital) method, *J. Comput. Chem. 21*, 1419−1432.
34. Vreven, T., Mennucci, B., da Silva, C. O., Morokuma, K., and Tomasi, J. (2001) The ONIOM-PCM method: combining the hybrid molecular orbital method and the polarizable continuum model for solvation. Application to the geometry and properties of a merocyanine in solution, *J. Chem. Phys. 115*, 62−72.
35. Vreven, T., Morkuma, K., Farakas, O., Schlegel, H. B., and Frish, M. J. (2003) Geometry optimization with QM/MM, ONIOM, and other combined methods. I. Microiterations and constraints, *J. Comput. Chem. 24*, 760−769.
36. Frisch, M. J., Trucks, G. W., Schlegel, H. B., Scuseria, G. E., Robb, M. A., Cheeseman, J. R., Montgomery, J. A., Jr., Vreven, T., Kudin, K. N., Burant, J. C., Millam, J. M., Iyengar, S. S., Tomasi, J., Barone, V., Mennucci, B., Cossi, M., Scalmani, G., Rega, N., Petersson, G. A., Nakatsuji, H., Hada, M., Ehara, M., Toyota, K., Fukuda, R., Hasegawa, J., Ishida, M., Nakajima, T., Honda, Y., Kitao, O., Nakai, H., Klene, M., Li, X., Knox, J. E., Hratchian, H. P., Cross, J. B., Bakken, V., Adamo, C., Jaramillo, J., Gomperts, R., Stratmann, R. E., Yazyev, O., Austin, A. J., Cammi, R., Pomelli, C., Ochterski, J. W., Ayala, P. Y., Morokuma, K., Voth, G. A., Salvador, P., Dannenberg, J. J., Zakrzewski, V. G., Dapprich, S., Daniels, A. D., Strain, M. C., Farkas, O., Malick, D. K., Rabuck, A. D., Raghavachari, K., Foresman, J. B., Ortiz, J. V., Cui, Q., Baboul, A. G., Clifford, S., Cioslowski, J., Stefanov, B. B., Liu, G., Liashenko, A., Piskorz, P., Komaromi, I., Martin, R. L., Fox, D. J., Keith, T., Al-Laham, M. A., Peng, C. Y., Nanayakkara, A., Challacombe, M., Gill, P. M. W., Johnson, B., Chen, W., Wong, M. W., Gonzalez, C., and Pople, J. A. (2003) *Gaussian 03*, revision C.02; Gaussian, Inc., Wallingford, CT.
37. Lee, C. T., Yang, W. T., and Parr, R. G. (1988) Development of the Colle-Salvetti correlation-energy formula into a functional of the electron density, *Phys. Rev. B 37*, 785−789.
38. Becke, A. D. (1993) Density-functional thermochemistry. 3. The role of exact exchange, *J. Chem. Phys. 98*, 5648−5652.
39. Cornell, W. D., Cieplak, P., Bayly, C. I., Gould, I. R., Merz, K. M. Jr., Ferguson, D. M., Spellmeyer, D. C., Fox, T., Caldwell, J. W., and Kollman, P. A. (1995) A second generation force field for the simulation of proteins, nucleic acids, and organic molecules, *J. Am. Chem. Soc. 117*, 5179−5197.
40. Hoops, S. C., Anderson, K. W., and Merz, K. M., Jr. (1991) Force field design for metalloproteins, *J. Am. Chem. Soc. 113*, 8262−8270.
41. Cieplak, P., Cornell, W. D., Bayly, C., and Kollman, P. A. (1995) Application of the multimolecule and multiconformational RESP methodology to biopolymers: charge derivation for DNA, RNA, and proteins, *J. Comput. Chem. 16*, 1357−1376.
42. Case, D. A., Pearlman, D. A., Caldwell, J. W., Cheatham, T. E., III, Wang, J., Ross, W. S., Simmerling, C. L., Darden, T. A., Merz, K. M., Stanton, R.V., Cheng, A. L., Vincent, J. J., Crow-ley, M., Tsui, V., Gohlke, H., Radmer, R. J., Duan, Y., Pitera, J., Massova, I., Seibel, G. L., Singh, U. C., Weiner, P. K., and Kollman, K. A. (2002) *AMBER*, University of California, San Francisco, CA.
43. Day, T. J., Soudackov, A. V., Cuma, M., Schmitt, U. W., and Voth, G. A. (2002) A second generation multistate empirical valence bond model for proton transport in aqueous systems, *J. Chem. Phys. 117*, 5839−5849.
44. Wang, J., Cieplak, P., and Kollman, P. A. (2000) How well does a restrained electrostatic potential (RESP) model perform in calculating conformational energies of organic and biological molecules? *J. Comput. Chem. 21*, 1049.
45. Kast, S. M., Nicklas, K. Bär, H.-J., and Brickmann, J. (1994) Constant temperature molecular dynamics simulations by means of a stochastic collision model. I. Noninteracting particles, *J. Chem. Phys. 100*, 566−576.
46. Hummer, G., Pratt, L. R., and Garcia, A. E. (1996) Free energy of ionic hydration, *J. Phys. Chem. 100*, 1206−1215.
47. Kumar, S., Bouzida, D., Swendsen, R. H., Kollman, P. A., and Rosenberg, J. M. (1992) The weighted histogram analysis method for free-energy calculations on biomolecules. I. The method, *J. Comput. Chem. 13*, 1011−1021.
48. Roux, B. (1995) The calculation of the potential of mean force using computer simulations, *Comput. Phys. Commun. 91*, 275−282.
49. Fisher, Z., Hernandez, Prada, J. A., Tu, C., Duda, D., Yoshioka, C., An, H., Govindasamy, L., Silverman, D. N., and McKenna, R. (2005) Structural and kinetic characterization of active-site histidine as a proton shuttle in catalysis by human carbonic anhydrase II, *Biochemistry 44*, 1097−1105.

50. Tu, C., Qian, M., Earnhardt, J. N., Laipis, P. J., and Silverman, D. N. (1998) Properties of intramolecular proton transport in carbonic anhydrase III, *Biophys. J. 74*, 3182−3189.
51. Fisher, Z. S., Maupin, C. M., Govindasamy, L., Budayova-Spano, M., Tu, C., Agbandje-McKenna, M., Silverman, D. N., Voth, G. A., and McKenna, R. (2006) Atomic crystal and molecular dynamics simulation structures of human carbonic anhydrase II: insights into the proton transfer mechanism, *Biochemistry 46*, 2930−2937.
52. Allen, T. W., Andersen, O. S., and Roux, B. (2004) Energetics of ion conduction through the gramacidin channel, *Proc. Natl. Acad. Sci. U.S.A. 101*, 117−122.
53. Gall, C. M., Cross, T. A., DiVerdi, J. A., and Opella, S. J. (1982) Protein dynamics by solid state NMR: the aromatic rings of the coat protein in fd, *Proc. Natl. Acad. Sci. U.S.A. 79*, 101−105.
54. Voth, G. A. (2006) Computer simulations of proton solvation and transport in aqueous and biomolecular systems, *Acc. Chem. Res. 39*, 143−150.
55. Humphrey, W., Dalke, A., and Schulten, K. (1996) VMD: visual molecular dynamics, *J. Mol. Graphics 14*, 33−38.
56. Merrit, E. A., and Murphy, M. E. P. (1994) Raster3D version 2.0: A program for photorealistic molecular graphics, *Acta Crystallogr., Sect. D 50*, 869−873.

BI062170F